IOP Publishing Journal Title
Journal **XX** (XXXX) XXXXXX https://doi.org/XXXX/XXXX

Using FDA-approved drugs as off-label fluorescent dyes for optical biopsies: from in silico design to ex vivo proof-of-concept

Michael C. Larson[1]*, Arthur F. Gmitro[1-3], Urs Utzinger[2-6], Andrew R. Rouse[1,3,7], Gregory J. Woodhead[1], Quinlan Carlson[8], Charles T. Hennemeyer[1], Jennifer K. Barton[1-5]†

1Medical Imaging, University of Arizona/Banner-University Medical Center.
2Biomedical Engineering Department, University of Arizona.
3College of Optical Sciences, University of Arizona.
4Electrical and Computer Engineering Department, University of Arizona.
5BIO5 Institute, University of Arizona.
6Obstetrics & Gynecology, University of Arizona/Banner-University Medical Center.
7Research, Innovation and Impact, University of Arizona.
8Post-Sophomore Fellowship in Pathology, College of Medicine, University of Arizona.
*To whom correspondence should be addressed: mikelarson@radiology.arizona.edu, 1501 N Campbell Ave., Tucson, Arizona 85724.
†Senior author.

Received xxxxxx
Accepted for publication xxxxxx
Published xxxxxx

Abstract

Optical biopsies bring the microscope to the patient rather than the tissue to the microscope, and may complement or replace the tissue-harvesting component of the traditional biopsy process with its associated risks. In general, optical biopsies are limited by the lack of endogenous tissue contrast and the small number of clinically approved *in vivo* dyes. This study tests multiple FDA-approved drugs that have structural similarity to research dyes, as off-label *in situ* fluorescent alternatives to standard *ex vivo* hematoxylin & eosin tissue stain. Numerous drug-dye combinations shown here may facilitate relatively safe and fast *in situ* or possibly *in vivo* staining of tissue, enabling real-time optical biopsies and other advanced microscopy technologies, which have implications for the speed and performance of tissue- and cellular-level diagnostics.

Keywords: fluorescence, optical biopsy, intravital microscopy, drug repurposing, fluorescence histopathology, fluorescent dyes, optical imaging

1. Introduction

Advancements in medical imaging technology have brought us closer to noninvasive disease diagnosis capabilities. However, obtaining a tissue sample for microscopic evaluation and diagnosis remains the gold standard for most disease states prior to therapy selection, as each (pharmacologic/chemotherapy, surgery, radiation, etc.) is associated with differences in risks, costs, and outcomes. As an example of the need for microscopic tissue evaluation, one study reported that MRI underestimated the diagnosis of cancer and pre-cancerous lesions by 25% when the purported findings in question were subsequently biopsied**[1]**. Thus, millions of people this year will have a biopsy, wherein a small piece of tissue is harvested for evaluation under a microscope, whether via image-guided needle biopsy**[2]**, biopsy performed during endoscopy**[3]**, or as a result of surgery.

The number of biopsies performed annually is growing, due to an aging population and the advent of precision medicine

with its associated demand for target tissue profiling**[2]**. Despite the minimally-invasive nature of needle and endoscopic biopsies, they are not without risks and limitations. Risks include pain, bleeding, and damage to the underlying tissue**[4]**, each organ having its unique complication (pneumothorax for lung biopsy, bowel perforation during endoscopic biopsy, etc.). Lastly, current needle biopsies are only macroscopically-guided, meaning that in a heterogeneous tissue conglomerate with portions of necrosis alongside normal, precancerous or cancerous cells, there is a risk of under-sampling pathologic changes. Tumor heterogeneity has been called the "limiting factor of precision medicine" in cancer care**[5]**. Incomplete tissue characterization can result in the need for additional biopsies, delay in care, or an imprecise or incorrect treatment strategy.

Optical biopsies, where the tissue under investigation is optically evaluated rather than physically harvested, could mitigate many of the risks and limitations of traditional biopsies, and decrease the costs and time of tissue processing before *ex vivo* microscopic evaluation. Since the mid 1980's when optical biopsy pioneers such as Dr. Robert Alfano distinguished cancer from benign tissue without processing tissue *ex vivo***[6,7]**, substantial progress has been made on the use of real-time optical techniques both on excised tissue and *in vivo*. Optical biopsy instruments, where the objective lens or optical fibers fit within a clinically-used laparoscope**[8,9]**, endoscope**[10]**, catheter**[11]**, or even down a hollow needle**[12,13]** are becoming progressively sophisticated and miniaturized, with seemingly exponential progress in technical innovations showcased annually**[14]**. Clinically, optical biopsies have been performed for over a decade during gastrointestinal (GI) endoscopy, with the clinical utility**[15]**, classification schemes**[16,17]**, and instrument vendors better described elsewhere**[18]**. These methods are also being applied to the lungs via bronchoscopy or in evaluation of pleural effusions**[19–21]**. Finally, optical biopsies outside of the aerodigestive tract are in the pre- to early clinical phase with promising but relatively limited data**[9,22–25]**.

While there are many ways to achieve tissue contrast in a histological specimen, a hematoxylin & eosin (H&E) stain is still by far the most used clinically**[26]**. H&E stain achieves differential coloring of cell nuclei from the cytoplasm and extracellular matrix. Numerous label-free optical imaging technologies demonstrate promising utility in providing unique contrast, including native autofluorescence **[6,7]**, Raman scattering **[27]** or optical harmonics **[28]** as a few examples. However, for over a century, H&E staining has enabled 70-80% of primary diagnoses based on tissue and cellular morphology without any additional special dyes or immunohistochemistry (IHC) **[29]**.

A growing number of slide-free optical imaging systems provide spatial resolutions that range from the organ to sub-cellular level**[30]**, a few which achieve H&E-type contrast although not *in vivo*. The closer such an optical biopsy system and resultant cellular contrast could approximate the traditional clinical H&E, the higher likelihood of clinical utility and successful adoption into clinical practice. The hypothesis of this study is that FDA-approved drugs that happen to fluoresce could be used off-label as alternative or complementary tissue and cellular dyes to produce an effect similar to routine H&E stains. Such drug-dye alternatives to an H&E (hereafter abbreviated as DDAs) would potentiate optical imaging technology to providing real-time diagnoses.

2. Methods

The goal of this study was to develop a combination of off-label drug-dyes as *in situ* and possible *in vivo* fluorescent stains easily visualized to better enable clinical optical biopsies. In summary, an exhaustive compilation of candidate DDAs was developed *in silico* from lists of 1) *in vivo* dyes used clinically mainly as diagnostic aids, and 2) from FDA-approved drugs with similar chemical structure to commonly-used fluorescent research dyes. The lists were then evaluated qualitatively as detailed in the supplemental section to generate a final possible set of drugs as off-label visibly fluorescent dyes. The initial DDA candidates were then tested *in vitro* via fluorescence spectroscopy and the list narrowed before finally testing them on tissue *ex vivo*/*in situ* using confocal microscopy.

In silico list of drug-dye candidates.

Supplemental Diagram 1 demonstrates the *in silico* workflow in developing possible DDAs. *In silico* evaluation began with compiling a list of known fluorescent or chromogenic dyes that stain the nucleus (similar to hematoxylin) and protein and cytoplasm (similar to eosin) in unfixed/intact cells.

DNA & Nuclear research dyes

A list of nuclear research dyes was generated from major vendor commercial websites, fluorophores.org, and through literature searches using keywords "DNA," "fluorescence," "fluorophore," "stain," and "dye." FDA-approved photosensitizing agents and chromoendoscopy dyes were also considered. Hematoxylin was excluded given its requiring a mordant for DNA staining**[26]**. Newer cell-impermeant DNA dyes (SYTOX family, TOTO/YOYO family), derivatives such as dimers (ethidium homodimer), linked fluorophores, or those otherwise modified for safety (Nancy-520, GelGreen, GelRed, EvaGreen, EZ-Vision®, SafeView™, RedSafe™, Midori Green Advance, GreenSafe Premium, SYBR® Safe), non-canonical DNA structure dyes,

RNA-specific dyes, and dyes with proprietary/unpublished structures (SYTO family) were excluded from analysis as the end goal is a Hematoxylin-equivalent nucleus stain, not simply staining of isolated nucleic acids as is done in gels/blots. Classical DNA dyes (ethidium, propidium, nuclear yellow) were included for comparison despite their semi-impermeability to intact cells.

The following are the research dyes evaluated, listed by DNA binding mechanism (*=classic or popular dye but semi/impermeable). Intercalators: 2**[31]**, 7-AAD (7-aminoactinomycin D)***[32]**, Acridine Orange**[8]**, AMCA (9-amino-6-chlor-2-methoxyacridine)**[32]**, BEBO/BETO/BOXTO**[32]**, BENA435**[33]**, "-OPRO's" (B/P/T/Y-OPRO)**[32]**, Dihydroethidium/hydroethidine/Ethidium*/Hexidium/Propidium***[32]**, DRAQ5**[34]**, DY-555 (representative of the DY family)**[35]**, EVOblue™ 30**[36]**, FOVPC2 (representative of the FOVPCx family)**[31,37]**, Imidazo-2**[31,35]**, PicoGreen***[38]**, SYBR Gold**[39]**, SYTO**[40]**, Thiazole Orange**[32]**; Groove binders: 1**[31]**, Chromomycin A3**[41]**, DAPI (4',6-diamidino-2-phenylindole)***[32]**, Hoechst's 33258, 33342, 34580**[32]**, P3**[31]**, RF1**[42]**, SYBR Green**[40]**, Nuclear yellow/Hoechst S769121**[32]**, TO3-CN**[43]**; Other/unknown DNA-binding mechanism: 3C2**[31,44]**, C61**[31,45]**, CHO3O-TO-CF3**[31]**, Hydroxystilbamidine**[32]**, LDS-751**[46]**, Z-TPE3**[31,47]**.

Structures of these DNA dyes were obtained from PubChem (https://pubchem.ncbi.nlm.nih.gov/, National Center for Biotechnology Information, Bethesda, MD, USA) and submitted to DrugBank.ca**[48]** for structural similarity search of approved compounds as of 2019 with a similarity score threshold arbitrarily set at 0.45. (The list of such drugs is included in Supplemental Table 1 alphabetical by the primary name used on DrugBank.ca).

Protein & cytoplasm research dyes

Eosins are known to fluoresce. Eosin-like molecules and other fluorescent molecules that could localize to the cytoplasm were found using search keywords "cytosol," "cytoplasm," "fluorescence," "fluorophore," "stain," and "dye." Fluorophores examined were Eosins (Bromoeosin, Eosin B, and Eosin Y), Calcein AM, MTT/Thiazolyl Blue, Resazurin**[49]**, 3-MTS, XTT, and ViaFluor® CFSE. Potential fluorophores that are primarily used for detecting reduction-oxidation reactions**[50]** were excluded (Peroxy Green 1, Peroxy Crimson 1, and Amplex Red).

In a similar manner to nuclear dyes, the protein and cytoplasm research dye structures were obtained from PubChem and submitted to DrugBank.ca for structural similarity search (Supplemental Table 2).

Clinical *in vivo* dyes:

FDA-approved visual contrast agents, such as vital dyes/chromophores**[51,52]** and fluorophores, were obtained by searching the literature including keywords of "in vivo," "intravital," "vital," "chromophore," "fluorophore," "visual," "fluorescent," or "dyes."

Protein-based drugs (BLZ-100) and drugs without current FDA approval per DrugBank.ca (bromophenol blue, bromsulphthalein, cresyl violet, Evan's blue, fast/light green, infracyanine green, Janus green B, Lissamine green, rhodamine 6G, tricarbocyanin, trypaflavin) were excluded from consideration.

Qualitative evaluation of DDA candidates.

Table 1 is the final list of top 20 drugs reviewed and considered for subsequent investigation as hematoxylin-like off-label drug-dyes based on their chemical structural similarity to research fluorophores. Table 2 contains a list of the top 14 drugs representing possible eosin-like off-label drug-dyes, also based on structural similarity to research dyes. (Only the top 14 eosin-equivalent dyes were evaluated as the 14th drug and many below it were also candidates for nuclear drug-dyes.) Table 3 is of actual *in vivo* chromophore/fluorophore drugs used clinically.

Assessment of these top similar drugs and clinical dyes was done 1) based on Lipinski's pharmacological "rule of 5" to evaluate off-label drug-dye candidates based on the assumption that optical biopsies will use topical or direct application, 2) considering the drug's known fluorescence spectra (requiring fluorescence emission in the visible wavelength), and 3) use and mechanism of action (and therefore presumed cellular localization). Details of such evaluation narrowing the possibilities are included in the supplemental section.

In vitro analysis

The resultant favorable drug-dyes were then evaluated *in vitro*. Congo red, indigo carmine, and phenol red were from Santa Cruz Biotechnology (Dallas, TX, USA); daunorubicin, fluorescein, methylene blue, mitoxantrone, phloxine B, rose bengal free acid were from Sigma-Aldrich (St. Louis, MO, USA); pyrvinium pamoate was from MedChemExpress (Monmouth Junction, NJ, USA). Pyrvinium pamoate was diluted in DMSO (Sigma-Adlrich, to a 1mM stock); all other drug-dyes were diluted in purified water to the concentration shown in each respective figure. Fluorescence spectroscopy was performed with drug-dyes diluted in deionized water to the concentration shown and evaluated on a Horiba Scientific Fluorolog 3 with 3nm slit width for excitation and 5nm slit emission scanning. Emission-excitation data was analyzed

using MATLAB as published previously**[53]**. Fluorescence spectroscopy of hematoxylin- and eosin-like combinations was done based on commonly-used excitation wavelengths, specifically 375nm, 405nm, 455nm, 488nm, and 532nm. For *in silico* analysis, the spectral requirement for *in vitro* evaluation was known emissions in the visible range. For *in vitro* evaluation for consideration of *ex vivo* analysis, we excluded drugs with excitation wavelengths in the UV range (below 380nm) and peak emissions above 700nm given the end goal of having a visible optical contrast panel. The need for UV excitation brings certain depth-of-penetration and safety constraints; and requiring infrared detectors, while certainly possible, would be less useful as stains detectable by the human eye, which is relatively less sensitive toward the edges of the visible spectrum than the mid-portion of the visible spectrum**[54]**.

In evaluating fluorescence compatibility *in vitro*, Spectragryph v1.2.11**[55]** (http://spectroscopy.ninja, Dr. Friedrich Menges, Oberstdorf, Germany) was used to remove Raman peaks, excitation harmonics peaks, normalize and smooth via triangular moving average data before presentation.

Supplemental methods and results contain a detailed description on the DDA candidates, including excitation-emission spectra. Supplemental Figure S1 is of excitation-emission spectragraphs of the candidate nuclear drug-dyes. Supplemental Figure S2 contains excitation-emission spectragraphs of the protein/cytoplasm dye candidates. Supplemental Figures S3 demonstrate technical factors needing consideration to optimize the emission spectra of combined DNA/nuclear- and protein/cytoplasm-dyes. Supplemental Figures S4 and S5 demonstrate varying degrees of compatibility between the potential DNA/nuclear- and protein/cytoplasm-dyes. Supplemental Figures S6-S10 are of normalized fluorescence emission spectra from the various potential optimized DDAs.

Ex vivo analysis

Confocal microscopy was done 1) to compare a commonly-used research dye with its most structurally-similar clinical drug using the exact same microscope settings and 2) to qualitatively evaluate the drug-dye combinations on *ex vivo* lung tissue. Microscopy was done on fresh bovine or ovine lung samples from the University of Arizona Food Products Safety Laboratory (depending on availability). Lung tissue samples approximately 2-3 hours after slaughter were initially kept in a sealed container at 4°C in air or either a sterile glucose-containing oral electrolyte solution (Parent's Choice™ Unflavored Pediatric Electrolyte Solution, Walmart, Bentonville, AR, USA) or Hank's Balanced Salt Solution (HBSS, Gibco Invitrogen, Carlsbad, CA, USA) overnight. The periphery of the tissue was trimmed to exclude any visibly crenated tissue. To evaluate for necrosis, 50µl of 0.4% toluidine blue was added to approximately 1 x 3 x 6 mm tissue samples, with minimal uptake seen at the periphery/pleural surface and along cut surfaces most prominently on tissue kept in HBSS (with 173 mean ±198 standard deviation positive cells per 10x objective/low-powered field of view, n=3), but minimal-to-none within the intact lung parenchyma in the oral electrolyte solution (70±80 positive cells per LPF) or air (26±21 trypan positive cells/LPF, images not shown). Subsequent tissue samples were only kept in air at 4°C overnight. All confocal microscopy was done on a Nikon Eclipse e600 microscope C1 confocal microscope system. Confocal microscopy of the samples was performed with excitation laser at 488nm wavelength on 515/30nm, 595/50nm, and 640nm/long pass channels (referred to as Channel 1, 2, and 3, respectively). For comparison of a research dye with its structurally-similar approved drug, microscopy settings were kept identical, with a dwell time of 3.60µsec per pixel and 1024 pixels per image (resulting in 636.5µm width and height of each image) and diffraction-limited imaging depth (pinhole size of 30µm). 20µM of either acridine orange (commonly-used research dye**[8]**) or proflavine (structurally-similar approved drug) were added to bovine lung tissues and imaged under the exact same microscope settings (Figure 1) after controlling for autofluorescence (Supplemental Figure 11).

Given that quantitative fluorescence imaging is fraught with difficulties**[56]** and not as important to the stated end goal as perception by a trained clinical observer, only semi-quantitative image analysis was performed.

Image analysis was done using ImageJ FIJI distribution**[57]** to manually trace 10 nuclei and the surrounding cytoplasm/background per image on 3 images of each of the research dye and similar drug (Supplemental Figure 12). Statistical analysis was done using one-way ANOVA for independent measures for intra-experimental verification of methods, including evaluation of the measured nucleus size in pixels (no difference with $F(1,59)=0.39$, $p=0.53$), signal ($F(1,59)=10.80$, $p=0.0017$), noise ($F(1,59)=14.98$, $p=0.00023$), and signal/noise ($F(1,59)=96.15$, $p<0.00001$).

DNA/nuclear and protein/cytoplasm drug-dyes, and combinations thereof, were added topically to *ex vivo* bovine and ovine lung tissue samples and imaged using confocal microscopy (Figures 3-6). For evaluation of DDA candidates, the confocal microscope settings were adjusted to optimize the resultant signal, with gains between 78-108 on Channel 1, 66-124 for Channel 2, and 68-94 for Channel 3, with otherwise identical dwell time, pixels per image, and image depth/width/height as above.

3. Results

Initial literature review and evaluation of potential drug-dye candidates.

Table 1 demonstrates the top 20 drugs by structural similarity to research nuclear dyes by drug class and DNA-binding mechanism. The complete list of drugs with structural similarity to research nuclear dyes (as defined in the Supplemental Methods section) can be seen on Supplemental Table S1. Table 2 shows the top 14 structurally-similar drugs to research cytoplasm dyes, also by drug class. The full list of drugs with similarity to the listed research dyes can be found on Supplemental Table S2. Supplemental Table S3 details clinically-used drugs for visible contrast, be they colored or fluorescent, and their general clinical use.

These top nuclear- and protein/cytoplasmic-drug dye possibilities were further evaluated based on their mechanism of action/cellular localization and fluorescence spectra if known as the final portion of *in silico* evaluation (as described below), and *in vitro* by fluorescence spectrophotometry (Supplemental Figures S1-S10).

Evaluation of lead drug-dye candidates.

A comparison was made between a drug and its structurally-similar research dye to prove the principle. Acridine orange (AO) is a well-known nucleus research dye**[8]**. It is very similar in structure to the topical anti-septic proflavine (Figure 1, insets) and acriflavine, a dye used outside of the United States of America for endoscopic optical biopsies**[17]**. Fifty microliters at 20μM of either AO or proflavine was topically applied to *ex vivo* but unprocessed and still *in situ* bovine lung tissue and imaged with confocal microscopy. Microscope settings were adjusted to minimize autofluorescence (Supplemental Figure S11) and kept identical between image acquisitions. Figure 1 demonstrates the resultant images comparing the research dye to the anti-septic drug. Supplemental Figure S11 is of the resultant tissue autofluorescence at the specific confocal microscope setting used to compare AO and proflavine. Supplemental Figure S12 demonstrates similarity of the FDA-approved drug relative to the research dye in terms of the resultant nuclear fluorescence signal and the signal/background.

Qualitative comparison of the proposed eosin-like non-specific protein/cytoplasmic dyes were performed. Fluorescein, phenol red, phloxine B, and rose bengal were each added to *ex vivo* bovine lung tissue and imaged under confocal microscopy (Figure 2).

The concentrations used with each cytoplasmic/protein drug-dye alternative (DDA) was intended to provide similar fluorescence intensity to subsequent addition of nuclear DDA. Each cytoplasmic/protein DDA resulted in variable staining of the proteinaceous connective tissue and cellular cytoplasm, granules or vesicles. Qualitatively at these concentrations, fluorescein, phloxine B and rose bengal DDA appeared best to localize to cell cytoplasm in addition to the connective tissue fibers. Such fibers also exhibited some autofluorescence at the same exposure time and intensity.

Combination fluorescent drug-dye alternatives to H&E on ex vivo lung tissue.

Various combinations of hematoxylin-like nuclear dyes and eosin-like protein/cytoplasmic dyes were next analyzed based on compatible fluorescence signal from a single excitation wavelength (and listed in alphabetical order by dye type, Supplemental Table S4).

Fluorescein was the only protein/cytoplasm dye without excessive overlap with the resultant fluorescence signal from daunorubicin as a nuclear dye (Supplemental Figure S6). This combination was added topically to ovine lung tissue and imaged using confocal microscopy. (Figure 3).

Methylene blue, as a pleiotropic drug and visual dye, was tested as a fluorescent DNA DDA using all the protein/cytoplasm dyes based on favorable fluorescent emission spectra (Supplemental Figure S7). These combinations were applied topically to ovine lung samples and imaged using confocal microscopy at 488nm excitation.

Mitoxantrone was used as a DNA dye in combination with all candidate protein/cytoplasm DDAs given their compatible fluorescence emission spectra (Supplemental Figure S8). Again, the combinations were topically applied to ovine lung and examined with confocal microscopy at 488nm excitation (Figure 5).

Lastly, proflavine and rose bengal had fluorescence emission characteristics amenable to a single wavelength of excitation (Supplemental Figure S9). The combination was tested on ovine lung samples and evaluated with confocal microscopy (Figure 6A). As the gold-standard for comparison to the DDAs, ovine lung tissue was fixed in formalin, embedded in paraffin and sectioned at 5μm thickness and finally stained with hematoxylin and eosin per routine protocol (Figure 6B).

Possible intralesional drug-dye combinations and concentrations relative to their typical clinical dose and route are shown in Supplemental Table S5. For the chemotherapeutics at this possible dosing, a very large intralesional injection would be 1% that of a therapeutic dose delivered systemically.

4. Discussion

Novel optical technologies utilizing native molecules optical properties, such as autofluorescence and absorption can provide dye-free tissue- and cellular-level detail, and the biological and clinical uses of such technology will undoubtedly expand. However, the addition of exogenous contrast agents can improve signal by orders of magnitude, enabling more rapid and/or specific image acquisition. Fluorescent drug-dye alternatives to traditional stains may facilitate the end goal of real-time clinical optical biopsies. In the case of DDAs approximating H&E, this would provide signal enhancement and/or decreasing the amount of time required to obtain images with nuclear and cytoplasmic contrast with clinically-acceptable signal to noise ratios. Further, this technique may also provide a way to microscopically guide physical biopsies to decrease inconclusive or false negative biopsies, or even possibly obviate the need for tissue harvest with its accompanying risks.

This study provides proof-of-concept from *in silico* design through *ex vivo/in situ* evaluation of clinical drugs for off-label use as fluorescent dyes as alternatives to H&E. The candidate dyes evaluated by this study replicate many qualities of traditional H&E staining, i.e., highlighting the nucleus similar to hematoxylin, and protein similar to eosin. Of the dyes tested, proflavine and rose bengal appeared to provide ideal nuclear and cytoplasmic/protein staining. However, as methylene blue and fluorescein are arguably the safest if given systemically, cheapest, and most accessible, this combination may also be top candidates to for further detailed study.

This study has several limitations. First, by its very nature as a proof of concept investigation, this study involved only application of stains to normal mammalian tissues *ex vivo*. Future studies will address the appearance of such drug-dyes in *in vivo* tissues, including diseased tissues such as with malignancy or infection. An additional limitation was that a single organ type was analyzed. The staining of a single tissue type is only an example, but does serve as a starting point. The lung was specifically chosen as the first organ to evaluate given that some of the authors are part of a different study to evaluate lung nodules with optical imaging at the time of a physical biopsy.

Additional limitations to the study include the following. The use of a single chemical structural similarity algorithm and drug database results in a fundamental limitation to the completeness of the resulting output. Narrowing the list of drugs with emission in visible wavelengths with a single excitation wavelength is a purposeful constraint given the goal is a visible DDA panel. However, if one were to do away with such constraints and use infrared detectors, optical filters, and multiple excitation wavelengths, multiplexing of H&E with other stain(s) and/or fluorescence IHC on the same tissue may even be possible. Evaluating only a single agent in a class such as anthracyclines (daunorubicin) and anthracenediones (mitoxantrone) provides proof-of-principle, but is a limitation to this study nonetheless. And while pamoates of themselves may be contributing to the broad fluorescence signal of pyrvinium pamoate resulting in unacceptable spectral overlap, it is the only formulation of pyrvinium currently in use according to DrugBank.ca at the time of this study, and is the formulation used in fluorescence research studies previously**[58]**.

Some of the DNA dyes are chemotherapeutic agents, which could appear as a clinical drawback to the use of such agents. However, the expected dosing of intralesional dyes for diagnostic optical imaging would be a fraction of, if not orders of magnitude lower than, the doses for therapeutic effect. For example, mitoxantrone is typically dosed systemically at 12mg/m^2 body surface area (totaling 20.4 mg for the average 1.7m^2 adult). A very large intralesional injection totaling 5ml of 100µM mitoxantrone (making 259µg) would be only 1% of a systemically-delivered therapeutic dose. Other chemotherapeutic DDAs with greater fluorescence efficiency may only need hundredths to thousandths of that required for a systemic therapeutic dose.

This proof-of-concept study raises multiple questions and avenues for future work. Could other drugs including photosensitizing drugs that didn't top the list in terms of structural similarity be used for this or other optical imaging indications? Which color additives and other dyes generally recognized as safe by the FDA, but not currently classified as drugs, could serve as alternatives to any number of histology stains such Gram, trichrome, Nissl, etc.? Answering such questions evaluating the additional 200+ drugs and 196 safe color-chemicals**[59]** would require further large-scale studies. Future studies will consider as candidate DDAs known chromophores, e.g. rifamycin and derivatives are known to cause orange-red staining of bodily tissue and fluids, and known fluorophores, e.g. tetracyclines are known to fluoresce **[60]**, despite their structural dissimilarity to research dyes for other possible staining indications.

Only semi-quantitative comparison of signal-to-background of an actual research dye to the DDA equivalent, as well as only qualitative comparison of the DDA to an actual H&E may be perceived limitations. However, the amount of time a piece of tissue is exposed to a staining solution, the concentration of the stain, the time and vigor of which the stain is washed and dried, use of counter-stains, and the temperature of all such solutions influences the resulting chromophore concentration in the tissue. The intensity of interrogating light and its component wavelengths coupled to the capabilities of the detector further influence the resulting

signal-to-noise. Thus, the same piece of tissue could have different signal-to-noise between subsequent H&E-stained slides. More meaningful measures for future studies include the qualitative acceptance by general pathologists, the time and confidence to arrive at a unique diagnosis comparing H&E and the DDAs, or comparative performance in an image analysis algorithm.

Other points to be addressed before widespread clinical use include 1) determining the optimal dosing, excitation wavelengths, and optical equipment for ideal image acquisition using DDAs; 2) understanding the dyes influence (if any) on actual H&E staining or other downstream specialized tissue testing should a physical biopsy be performed, and if so, at what concentration and to what depth and in which tissue types; and 3) issues for clinicians and pathologists to store and interpret the resultant images. Clearly, more work has to be done before the possibilities demonstrated here become accepted as a true alternative to H&E stains.

What we labeled as incompatible nuclear DDAs and protein/cytoplasm DDAs was defined in part with simplicity (single excitation wavelength and use of off-the-shelf optical equipment) in mind. Fluorescein and daunorubicin did have substantial emission overlap when excited at 488, but the overlap was not in all detection channels used in our confocal studies. Other experiments using multiple excitation wavelengths or different optical filters could prove that such "incompatible" or marginally-compatible combinations actually work well, but this does not detract from the proof-of-principle this study provides.

Despite these remaining questions and limitations, the results of this study can theoretically be applied instantly to many of the novel optical imaging tools**[30,34]**, both for *in vivo* use and as potentially safer and/or less costly alternatives to *ex vivo* dyes. For example, the use of methylene blue and fluorescein with similar emission peaks as DRAQ5 and eosin, respectively, could potentially be used as dyes in a novel slide-free histology technique**[34]**. Also, the DDAs in this study have potential for immediate clinical application for fluorescent endoscopy or microscopy of any type, be it upper endoscopy, bronchoscopy, colonoscopy, etc. as physicians are able to use drugs off-label if it is in their professional judgment that benefits would outweigh possible risks**[61]**.

The real-time staining of unprocessed tissue applied *in vivo* could revolutionize "digital pathology," which now consists of the fairly indirect digital image capture of an already-processed and stained thin slice of tissue on a glass slide. "Direct digital pathology" where the stain is applied and images are acquired *in vivo* would allow for instant determination of cancer-or-not in certain situations such as with fungal lung nodules. Such optical biopsies would also allow for repeated sampling of the same region of tissue under image guidance when conventional imaging is equivocal or otherwise unhelpful (e.g. in 18-FDG negative cancers without a liquid biopsy/relevant biomarker to follow). Additionally, one pass of a clinical optical biopsy needle could replace fine needle aspirations, where a small needle is passed in and out of a lesion multiple times to harvest loose cells for subsequent staining and evaluation. With the growing need for tumor tissue for molecular profiling and precision medicine, optical biopsy technology could provide cellular-level imaging guidance of a physical biopsy to decrease false-negatives or non-diagnostic samples. Optical needle biopsies may also offer a slightly less invasive way to evaluate at the cellular level end-stage diseased or transplanted organs, or minimize the collateral damage associated with central nervous system or other critical organ biopsies.

5. Conclusion:

This study provides proof-of-concept for the off-label use of FDA-approved drugs as dyes for in situ clinical microscopy, a possible complement or alternative to traditional biopsy and routine tissue staining.

While a clinical trial of the DDA combinations may ultimately be needed before use of such agents for optical biopsy/real-time *in vivo* microscopy, this study demonstrates an avenue for future research and possible immediate use of drugs that happen to fluoresce as contrast agents in clinical microscopy/optical imaging, widening the bottleneck between leading edge optical technology and cellular-level clinical diagnostics.

6. Figures, tables and diagrams:

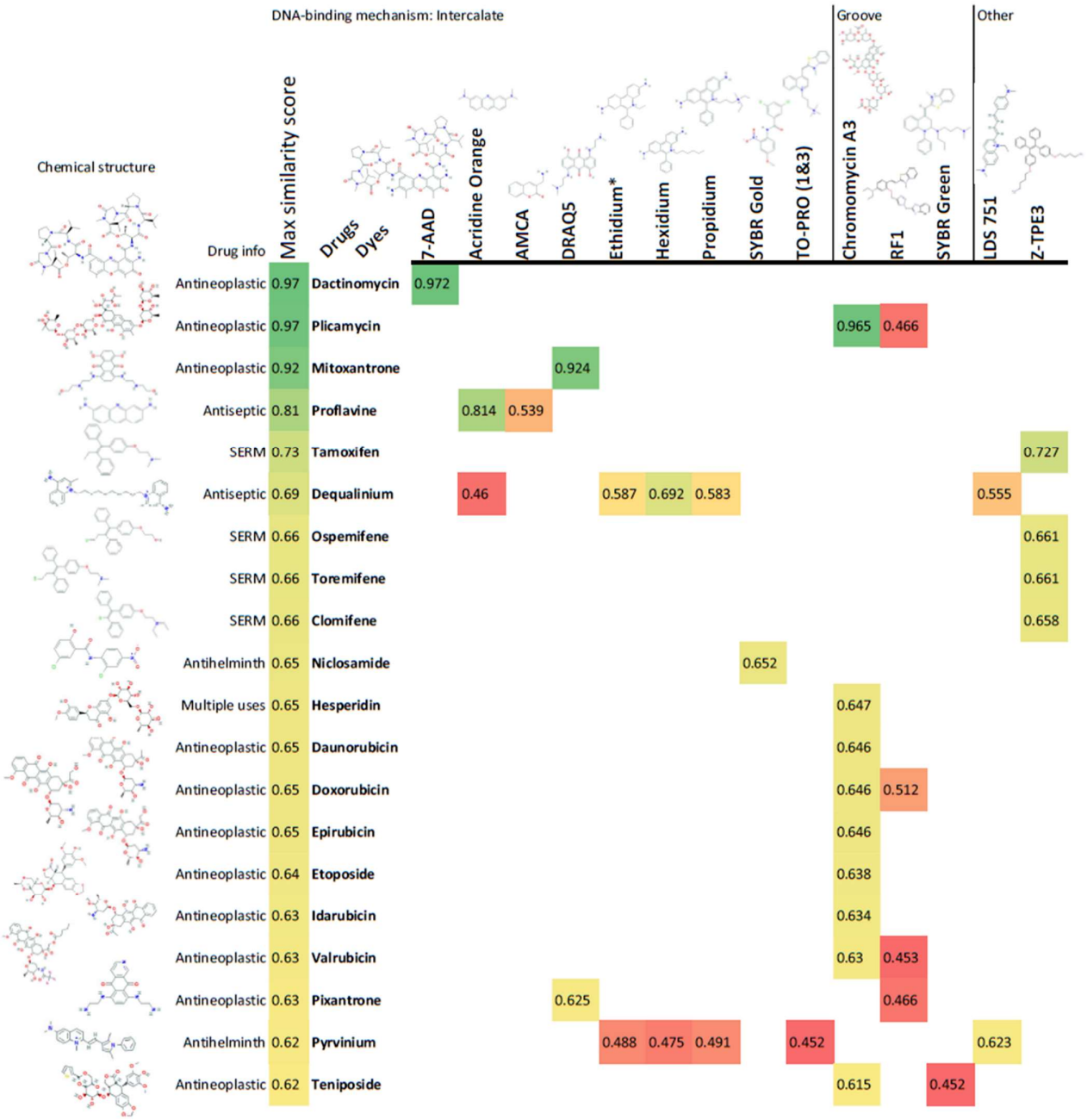

Table 1: Top 20 FDA-approved drugs with structural similarity to non-approved research nuclear dyes (by DNA-binding mechanism, on top). Drugs are sorted based on the maximum similarity score to research dye(s) with the color representing a higher to lower similarity from green to yellow to red; * indicates classic (semi-)impermeable cell stain for comparison. SERM, selective estrogen receptor modulator; see materials and methods section for dye chemical name acronym explanations.

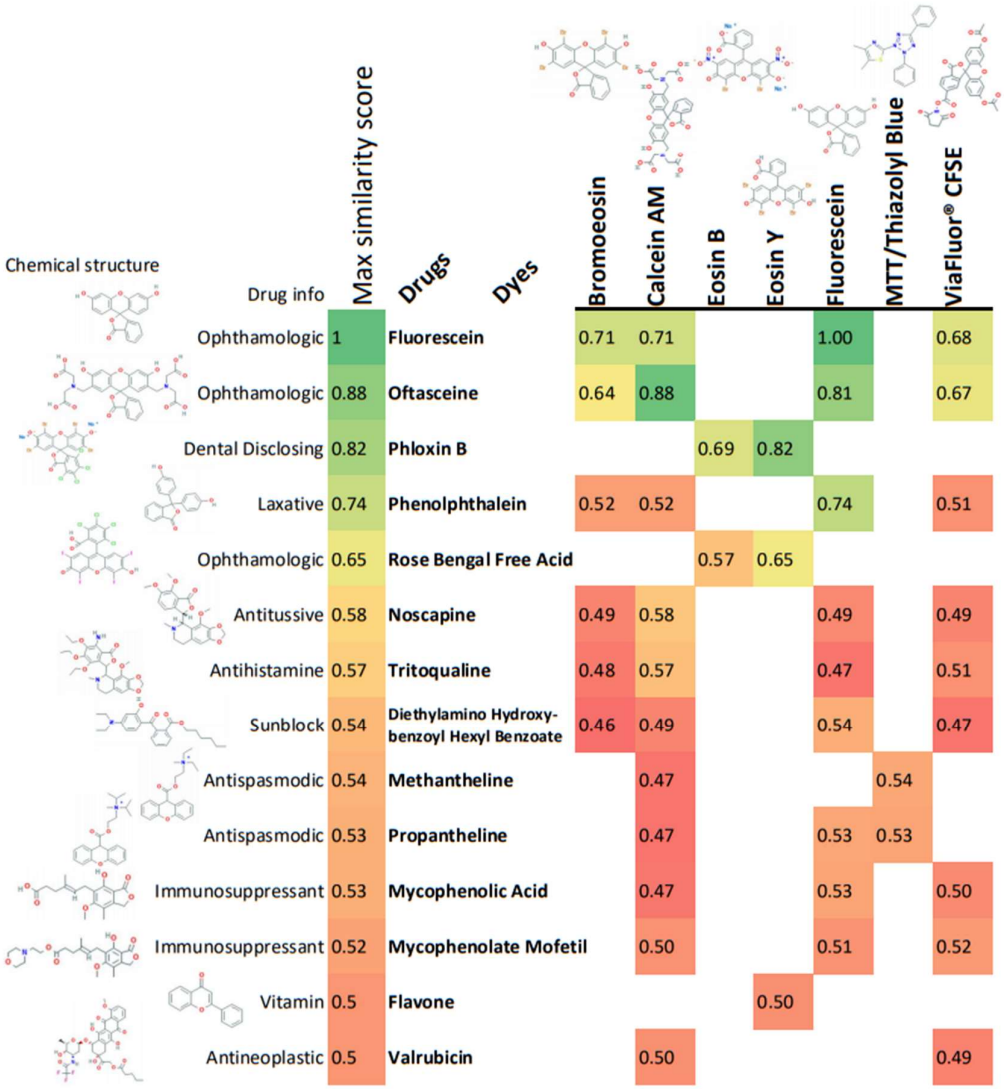

Table 2: Top 14 FDA-approved drugs with structural similarity to non-approved research cytoplasmic dyes. Drugs are sorted based on the maximum similarity score to research dye(s) with the color representing a higher to lower similarity from green to red. Only the top 14 were shown as drugs lower on the list showed similarity to nuclear dyes (e.g. drug number 14 on Table 2, Valrubicin as a known DNA-binding molecule, was also number 17 on Table 1).

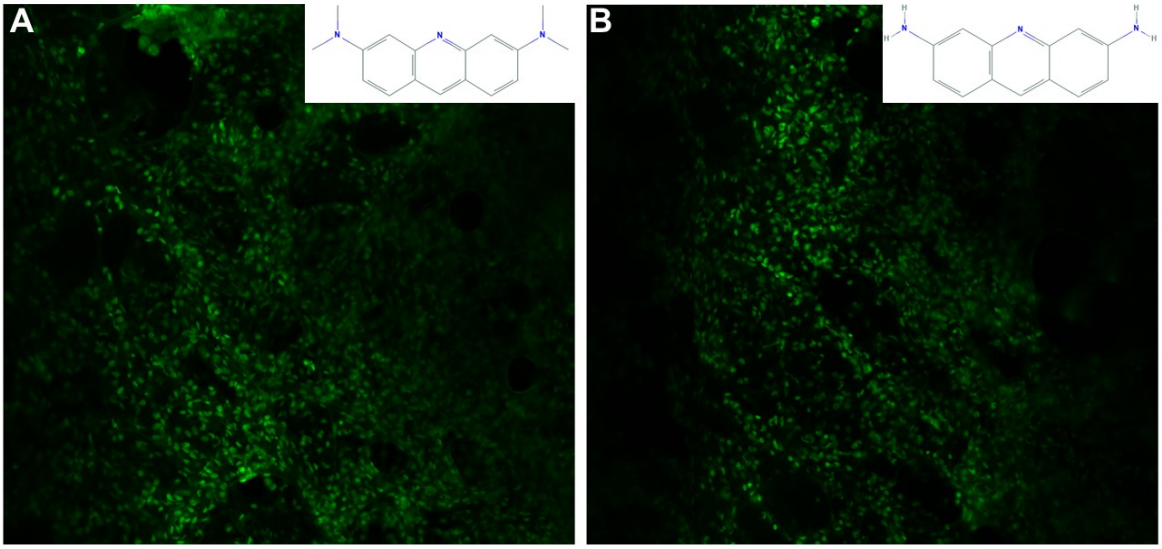

Figure 1: Proof-of-concept comparison of nuclear research dye with structurally-similar drug-dye. Representative images of (A) acridine orange (AO), a research nuclear dye, staining bovine lung tissue *ex vivo* and imaged with confocal microscopy. Inset shows the chemical structure of AO. (B) Proflavine, an approved topical antiseptic and wound irrigant, was placed on a similar-sized tissue sample and imaged with the exact same microscope settings. Inset is the structure of proflavine. 50µl at 20µM concentration of either dye was applied topically and then immediately imaged. Qualitatively and semi-quantitatively, the drug (proflavine) highlighted the nucleus as well as or better than the research dye, AO (see supplemental material). Image fields are 635.5µm in height x width.

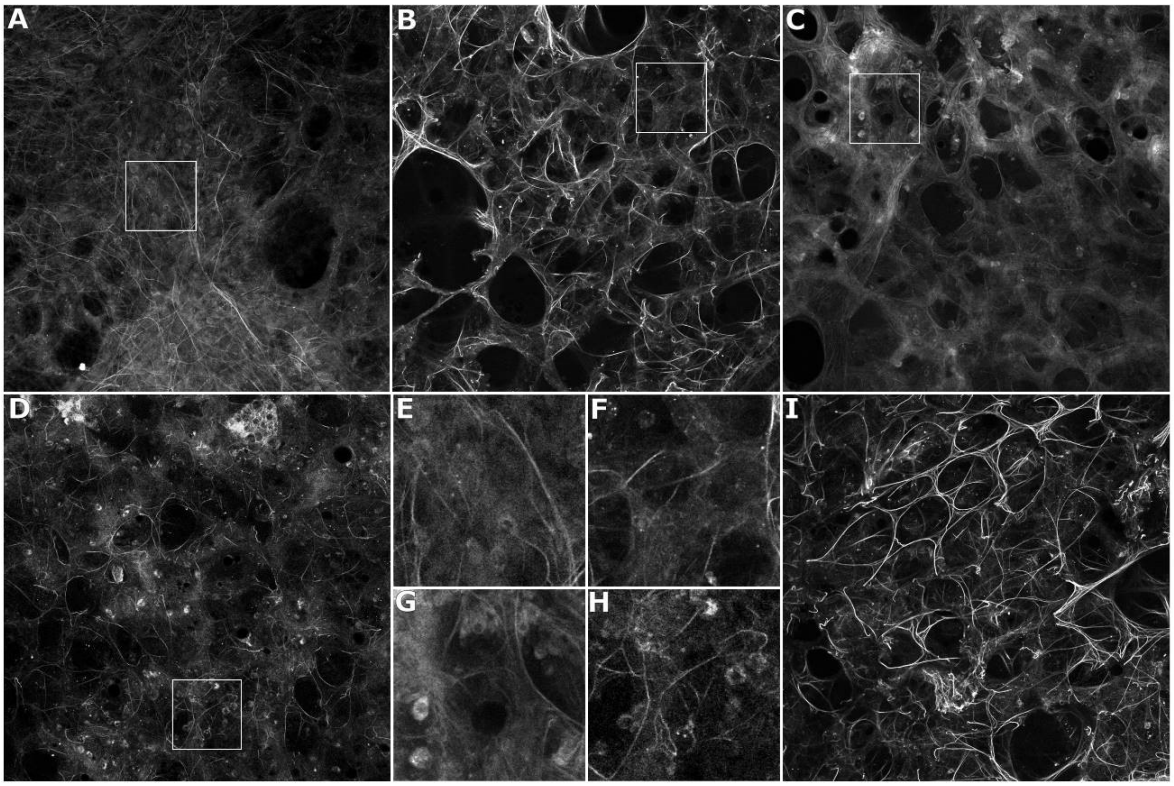

Figure 2: Comparison of various protein & cytoplasm dyes. (A) Fluorescein 500nM, (B) phenol red 100µM, (C) phloxine B 10µM, or (D) rose bengal 100µM in 50µL were all placed directly on bovine lung tissue and imaged using confocal microscopy excited with 488nm wavelength at various gains but otherwise identical exposure times and resolution (with 30µm pinhole, 20X/0.5 numerical aperture objective). Inset from (E) fluorescein, (F) phenol red, (G) phloxine B, and (H) rose bengal showing fluorescence signal includes signal from fibers and variable cellular uptake. (I) Optimized autofluorescence signal demonstrates prominent fibers but relative lack of cellular signal. Brightness/contrast was adjusted after acquisition, with no change in the gamma on any images. Image fields of A-D and I are each 636µm wide x tall. Image fields of E-H are 112µm wide x tall.

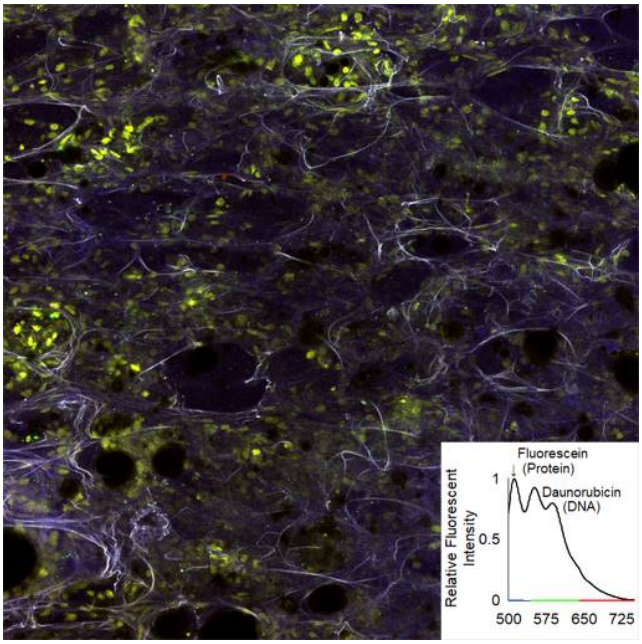

Figure 3: Daunorubicin and fluorescein as DNA and protein/cytoplasm dyes, respectively. The combination of 25µM daunorubicin and 250nM fluorescein was added to ovine lung tissue samples and imaged using confocal microscopy with 488nm excitation and imaged field being 636.5µm, with all microscope settings as in Figure 2 (except varying gain/brightness). Inset shows emission wavelength of the combination at 488nm excitation with the microscope channels indicated along the abscissa. Blue false-color: fluorescein. Yellow (green + red) false-color: daunorubicin.

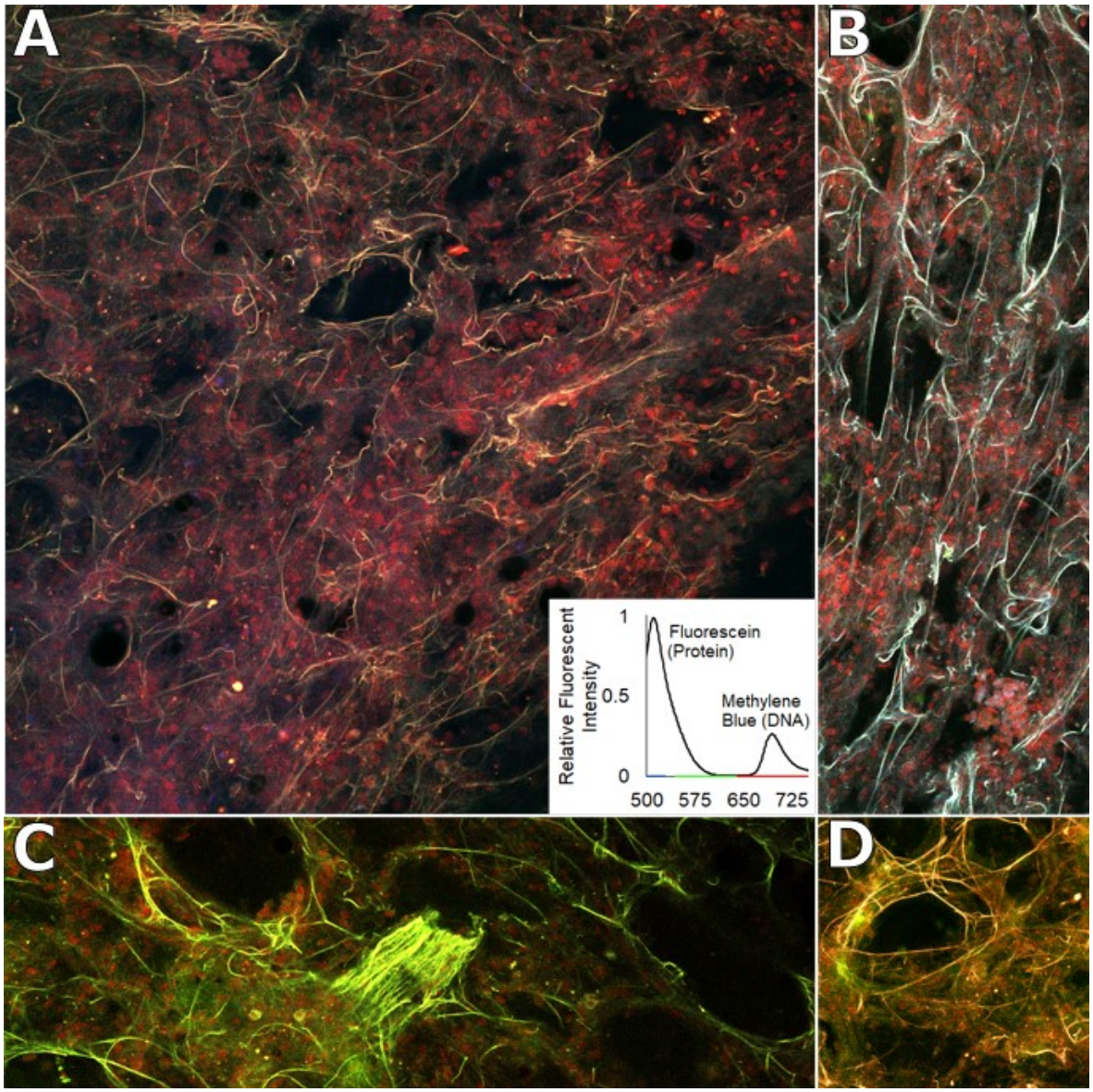

Figure 4: Methylene blue as a DNA dye with off-label protein/cytoplasm dyes. Methylene blue and the various protein/cytoplasm dyes were added in combination to ovine lung samples and imaged using confocal microscopy. (A) 50µM Methylene blue with 250nM fluorescein, with yellow (blue + green) false-color from fluorescein, and red from methylene blue. (B) 100µM Methylene blue with 100µM phenol red, with cyan (blue + green) from phenol red, and red from methylene blue. (C) 100µM Methylene blue with 10µM phloxine B, and green from phloxine B and red from methylene blue. (D) 100µM Methylene blue with 100µM rose bengal, with resultant green-yellow from rose bengal and red from methylene blue. All images had identical exposure times and resolution, with image fields of 636.5µm wide x tall, but with varying gain/brightness. Insets show fluorescence emission spectra of the respective combination in similar concentration ratios also at 488nm excitation, again with the microscope detector channels along the abscissa.

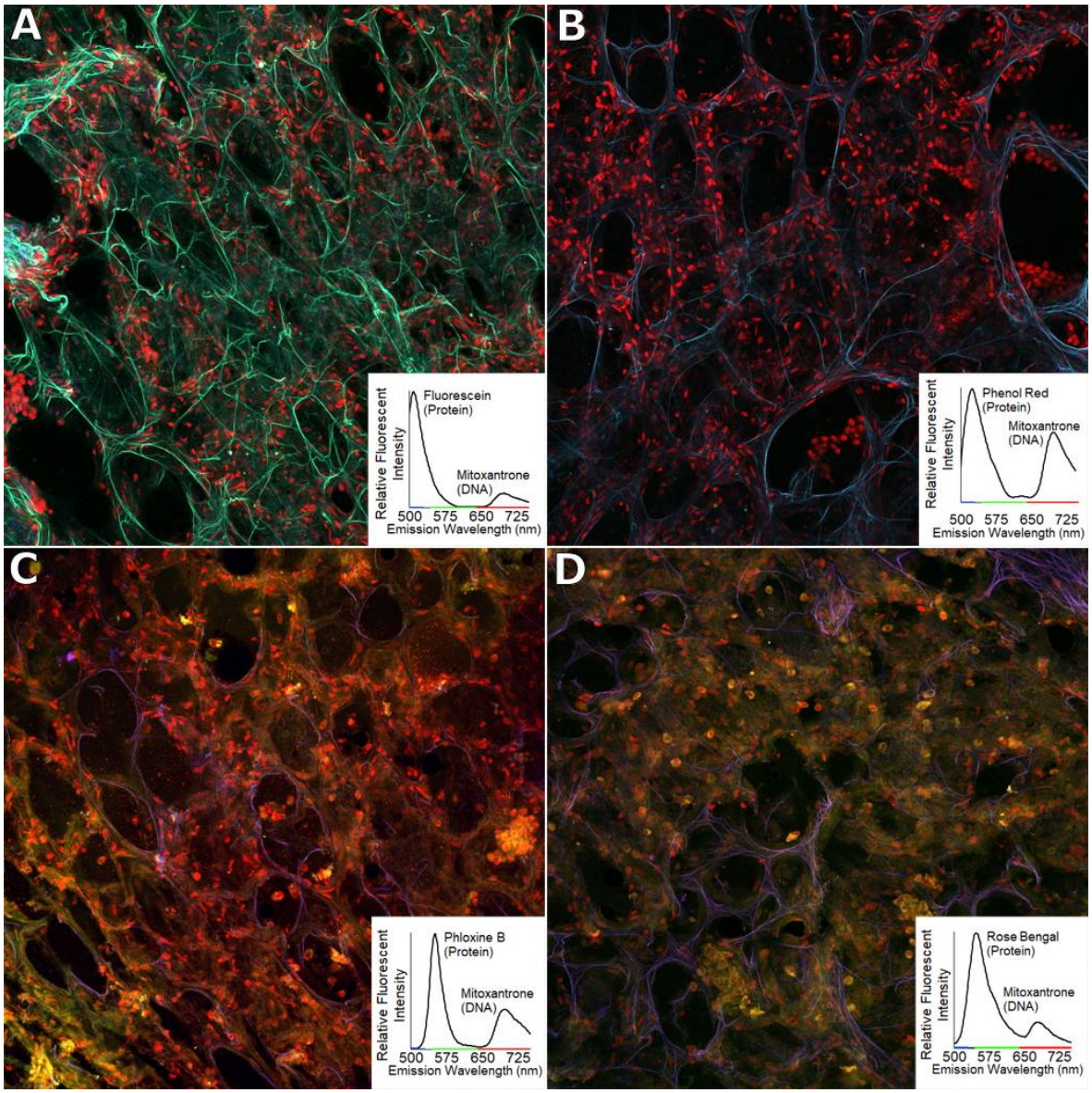

Figure 5: Mitoxantrone as a DNA drug-dye with the candidate protein/cytoplasm drug-dyes. Mitoxantrone and the protein/cytoplasm drug-dye candidates were topically applied to ovine lung samples and imaged with confocal microscopy. (A) Mitoxantrone 50µM and fluorescein 250nM, with cyan (blue + green channels) representing fluorescein signal, and red showing Mitoxantrone. (B) Mitoxantrone at 100µM and phenol red 100µM, with blue demonstrating phenol red staining, and red from mitoxantrone. (C) Mitoxantrone 50µM and phloxine B 50µM, with yellow false-color from phloxine B, and red from mitoxantrone. (D) Mitoxantrone 100µ and rose bengal 100µM with false-colored blue + yellow from rose bengal and red from mitoxantrone. All confocal microscopy images were from 488nm excitation and image fields and 636.5µm at settings identical to those in Figure 2 (excepting optimized brightness/gain across the different channels). Insets show fluorescence emission spectra of the respective combination in similar ratios also at 488nm excitation.

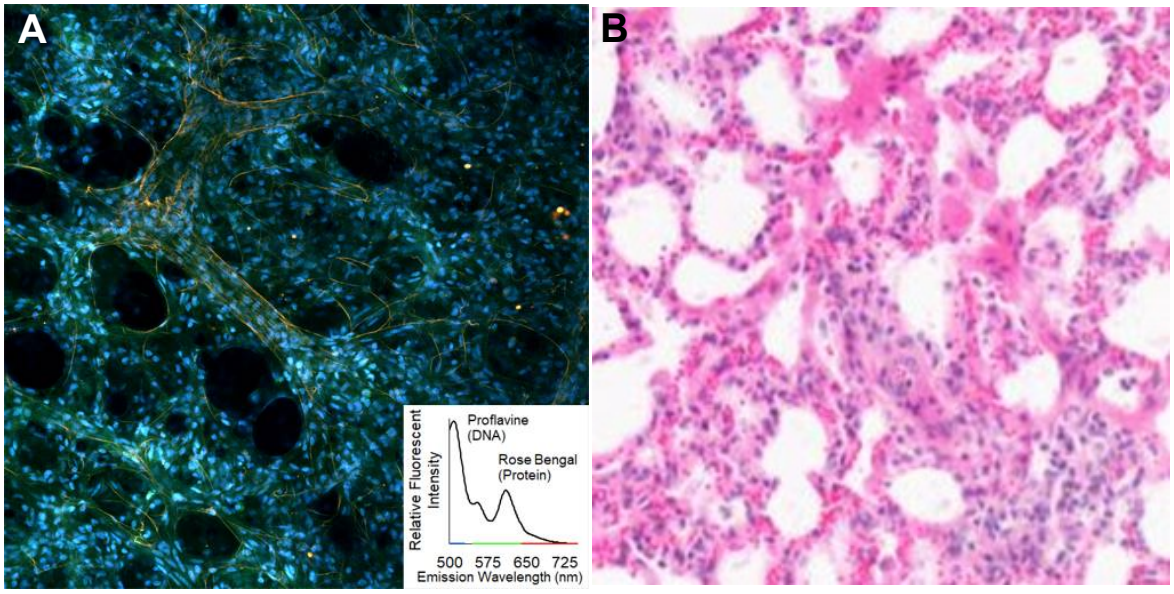

Figure 6: Proflavine as a DNA DDA with rose bengal as a protein/cytoplasm DDA, and hematoxylin and eosin-stained tissue for comparison. (A) 50µl of 100µM Proflavine and 100µM Rose Bengal was pipetted upon ovine tissue ex vivo and examined under confocal microscopy with a 488nm laser with imaged fields being 635.5µm; blue is false-colored proflavine signal, and green from rose bengal. Inset shows the fluorescence emission spectrum of the combination at 488nm excitation. (B) Ovine lung tissue was fixed in 10% formalin, paraffin embedded, cut to 5µm sections and stained with hematoxylin and eosin per routine protocol, then imaged at 20X with image field at also 636µm.

Acknowledgements

The data that support the findings of this study are available upon reasonable request from the authors.

The authors would like to thank the American Board of Radiology for granting M.C.L. a position on the B. Leonard Holman Research Residency track, which enabled this work. The authors would also like to thank Reed's Compounding Pharmacy of Tucson, AZ, USA, for providing clinical chemicals near their expiration date for testing (though none of the provided chemicals ended up in use for this paper).

Funding: Cook Medical Cesare Gianturco/RSNA Research Resident Grant RR1936 to M.C.L. for Furthering the Foundation of Clinical Optical Biopsies.

University of Arizona Cancer Center Cancer Imaging Program Harrison H. and Catherine C. Barrett and the Technology Research Initiative Fund Grant to C.T.H. and A.R.R. for Clinical Use of Confocal Microscopy to Differentiate Coccidiomycosis from Lung Cancer During Minimally Invasive Needle Biopsy.

Author contributions: M.C.L., C.T.H., A.R.R, A.F.G. and J.K.B. all helped conceived portions of the study. Spectral analysis was conducted in the U.U. laboratory. U.U contributed code for illustration of the spectra. A.F.G. assisted M.C.L. in confocal microscope data collection. M.C.L. performed the *in silico* and *in vitro*. All authors critically analyzed and edited the manuscript.

Competing interests: M.C.L. and C.T.H. are co-founders of a novel physical biopsy device start-up company and have conflict of interest management plans in place. UArizona has filed a provisional regarding drug-dye combinations.

References

[1] Verheyden C, Pages-Bouic E, Balleyguier C, Cherel P, Lepori D, Laffargue G, Doutriaux I, Jalaguier A, Poncelet E, Millet I, Thomassin-Naggara I and Taourel P 2016 Underestimation Rate at MR Imaging-guided Vacuum-assisted Breast Biopsy: A Multi-Institutional Retrospective Study of 1509 Breast Biopsies *Radiology* **281** 708–19

[2] Kwan S W, Bhargavan M, Kerlan R K and Sunshine J H 2010 Effect of advanced imaging technology on how biopsies are done and who does them *Radiology* **256** 751–8

[3] Kavic S M and Basson M D 2001 Complications of endoscopy *The American Journal of Surgery* **181** 319–32

[4] Nicholson M L, Wheatley T J, Doughman T M, White S A, Morgan J D, Veitch P S and Furness P N 2000 A prospective randomized trial of three different sizes of core-cutting needle for renal transplant biopsy. *Kidney Int* **58** 390–5

[5] Coyne G O, Takebe N and Chen A P 2017 Defining precision: The precision medicine initiative trials NCI-MPACT and NCI-MATCH *Current Problems in Cancer* **41** 182–93

[6] Alfano R, Tata D, Cordero J, Tomashefsky P, Longo F and Alfano M 1984 Laser induced fluorescence spectroscopy from native cancerous and normal tissue *IEEE Journal of Quantum Electronics* **20** 1507–11

[7] Alfano R, Tang G, Pradhan A, Lam W, Choy D and Opher E 1987 Fluorescence spectra from cancerous and normal human breast and lung tissues *IEEE Journal of Quantum Electronics* **23** 1806–11

[8] Tanbakuchi A A, Rouse A R, Hatch K D and Gmitro A F 2009 Clinical results with acridine orange using a novel confocal laparoscope *Progress in Biomedical Optics and Imaging - Proceedings of SPIE* Endoscopic Microscopy IV p 71720H

[9] Chene G, Chauvy L, Buenerd A, Moret S, Nadaud B, Beaufils E, Le Bail-Carval K, Chabert P, Mellier G and Lamblin G 2017 In vivo confocal laser endomicroscopy during laparoscopy for gynecological surgery: A promising tool *Journal of Gynecology Obstetrics and Human Reproduction* **46** 565–9

[10] Keenan M, Tate T H, Kieu K, Black J F, Utzinger U and Barton J K 2016 Design and characterization of a combined OCT and wide field imaging falloposcope for ovarian cancer detection *Biomed Opt Express* **8** 124–36

[11] Kim J B, Park K, Ryu J, Lee J J, Lee M W, Cho H S, Nam H S, Park O K, Song J W, Kim T S, Oh D J, Gweon D, Oh W-Y, Yoo H and Kim J W 2016 Intravascular optical imaging of high-risk plaques in vivo by targeting macrophage mannose receptors *Sci Rep* **6**

[12] Kano A, Rouse A R and Gmitro A F 2013 Ultrathin single-channel fiberscopes for biomedical imaging *J Biomed Opt* **18** 16013

[13] Landau S M, Liang C, Kester R T, Tkaczyk T S and Descour M R 2010 Design and evaluation of an ultra-slim objective for in-vivo deep optical biopsy *Opt Express* **18** 4758–75

[14] Alfano R R, Demos S G and Seddon A B 2021 Optical Biopsy XIX: Toward Real-Time Spectroscopic Imaging and Diagnosis Photonics West (SPIE)

[15] Fugazza A, Gaiani F, Carra M C, Brunetti F, Lévy M, Sobhani I, Azoulay D, Catena F, de'Angelis G L and de'Angelis N 2016 Confocal Laser Endomicroscopy in Gastrointestinal and Pancreatobiliary Diseases: A Systematic Review and Meta-Analysis *BioMed Research International*

[16] Wallace M, Lauwers G Y, Chen Y, Dekker E, Fockens P, Sharma P and Meining A 2011 Miami classification for probe-based confocal laser endomicroscopy *Endoscopy* **43** 882–91

[17] Kiesslich R, Burg J, Vieth M, Gnaendiger J, Enders M, Delaney P, Polglase A, McLaren W, Janell D,

Thomas S, Nafe B, Galle P R and Neurath M F 2004 Confocal laser endoscopy for diagnosing intraepithelial neoplasias and colorectal cancer in vivo *Gastroenterology* **127** 706–13

[18] Chauhan S S, Dayyeh B K A, Bhat Y M, Gottlieb K T, Hwang J H, Komanduri S, Konda V, Lo S K, Manfredi M A, Maple J T, Murad F M, Siddiqui U D, Banerjee S and Wallace M B 2014 Confocal laser endomicroscopy *Gastrointestinal Endoscopy* **80** 928–38

[19] Su Z, Zhong C, Li S, Chen X, Chen Y and Tang C 2017 Needle-based confocal laser endomicroscopy in the diagnosis of peripheral pulmonary nodule: a preliminary report *J Thorac Dis* **9** 2608–12

[20] Wijmans L, de Bruin D M, Meijer S L and Annema J T 2016 Real-Time Optical Biopsy of Lung Cancer *Am J Respir Crit Care Med* **194** e10–1

[21] Zirlik S, Hildner K, Rieker R J, Vieth M, Neurath M F and Fuchs F S 2018 Confocal Laser Endomicroscopy for Diagnosing Malignant Pleural Effusions *Med Sci Monit* **24** 5437–47

[22] Brunckhorst O, Ong Q J, Elson D and Mayer E 2019 Novel real-time optical imaging modalities for the detection of neoplastic lesions in urology: a systematic review *Surg Endosc* **33** 1349–67

[23] Werahera P N, Jasion E A, Liu Y, Daily J W, Arangua P, Jones C, Nash S R, Morrell M and Crawford E D 2015 Human feasibility study of fluorescence spectroscopy guided optical biopsy needle for prostate cancer diagnosis *Conf Proc IEEE Eng Med Biol Soc* **2015** 7358–61

[24] Kim J K, Choi J W and Yun S H 2013 Optical fine-needle imaging biopsy of the brain *Biomed Opt Express* **4** 2846–54

[25] Ramakonar H H 2017 220 A Stereotactic Brain Biopsy Needle Integrating an Optical Coherence Tomography (OCT) Probe with Blood Vessel Detection in Human Patients *Neurosurgery* **64** 260–260

[26] Titford M 2005 The long history of hematoxylin *Biotech Histochem* **80** 73–8

[27] Zhou Y, Liu C, Li J, Li Z, Zhou L, Chen K, Pu Y, He Y, Zhu K, Li Q and Alfano R R 2014 Tumor margin detection using optical biopsy techniques *Optical Biopsy XII* vol 8940, ed R R Alfano and S G Demos (SPIE) pp 153–7

[28] Sun C-K, Chen C-C, Chu S-W, Tsai T-H, Chen Y-C and Lin B-L 2003 Multiharmonic-generation biopsy of skin *Optics letters* **28** 2488–90

[29] Gupta S, Kundra V, Lam V and Kalhor N 2019 Requirements for Tumor Biopsies in the Age of Precision Cancer Care

[30] You S, Sun Y, Chaney E J, Zhao Y, Chen J, Boppart S A and Tu H 2018 Slide-free virtual histochemistry (Part II): detection of field cancerization *Biomed Opt Express* **9** 5253–68

[31] Suseela Y V, Narayanaswamy N, Pratihar S and Govindaraju T 2018 Far-red fluorescent probes for canonical and non-canonical nucleic acid structures: current progress and future implications *Chem Soc Rev* **47** 1098–131

[32] Wiederschain G 2011 The Molecular Probes handbook. A guide to fluorescent probes and labeling technologies *Biochemistry (Moscow)* **76** 1276–1276

[33] Erve A, Saoudi Y, Thirot S, Guetta-Landras C, Florent J-C, Nguyen C-H, Grierson D S and Popov A V 2006 BENA435, a new cell-permeant photoactivated green fluorescent DNA probe *Nucleic Acids Res.* **34** e43

[34] Elfer K N, Sholl A B, Wang M, Tulman D B, Mandava S H, Lee B R and Brown J Q 2016 DRAQ5 and Eosin ('D&E') as an Analog to Hematoxylin and Eosin for Rapid Fluorescence Histology of Fresh Tissues *PLOS ONE* **11** e0165530

[35] Linck L, Kapusta P and Resch-Genger U 2012 Spectroscopic and photophysical properties of dUTP and internally DNA bound fluorophores for

optimized signal detection in biological formats *Photochem. Photobiol.* **88** 867–75

[36] Buschmann V, Weston K D and Sauer M 2003 Spectroscopic Study and Evaluation of Red-Absorbing Fluorescent Dyes *Bioconjugate Chem.* **14** 195–204

[37] Chi S, Li L and Wu Y 2016 Photostability Enhancement of Fluorenone-Based Two-Photon Fluorescent Probes for Cellular Nucleus Monitoring and Imaging *J. Phys. Chem. C* **120** 13706–15

[38] Dragan A I, Casas-Finet J R, Bishop E S, Strouse R J, Schenerman M A and Geddes C D 2010 Characterization of PicoGreen interaction with dsDNA and the origin of its fluorescence enhancement upon binding *Biophys. J.* **99** 3010–9

[39] Guzaev M, Li X, Park C, Leung W-Y and Roberts L 2017 Comparison of Nucleic Acid Gel Stains Cell permeability, safety, and sensitivity of ethidium bromide alternatives *Biotium, Inc.* 1–4

[40] Deligeorgiev T G, Kaloyanova S and Vaquero J J 2009 Intercalating Cyanine Dyes for Nucleic Acid Detection *Recent Patents on Materials Science* **2** 26

[41] Chakrabarti S, Dasgupta D and Bhattacharyya D 2000 Role of mg2+ in chromomycin a3 - DNA interaction: a molecular modeling study *J Biol Phys* **26** 203–18

[42] Gaur P, Kumar A, Dalal R, Bhattacharyya S and Ghosh S 2017 Emergence through delicate balance between the steric factor and molecular orientation: a highly bright and photostable DNA marker for real-time monitoring of cell growth dynamics *Chem. Commun. (Camb.)* **53** 2571–4

[43] Zhang S, Fan J, Li Z, Hao N, Cao J, Wu T, Wang J and Peng X 2014 A bright red fluorescent cyanine dye for live-cell nucleic acid imaging, with high photostability and a large Stokes shift *J. Mater. Chem. B* **2** 2688–93

[44] Kwon S, Kwon D I, Jung Y, Kim J H, Lee Y, Lim B, Kim I and Lee J 2017 Indolizino[3,2-c]quinolines as environment-sensitive fluorescent light-up probes for targeted live cell imaging *Sensors and Actuators B: Chemical* **252** 340–52

[45] Feng S, Kim Y K, Yang S and Chang Y-T 2010 Discovery of a green DNA probe for live-cell imaging *Chem. Commun. (Camb.)* **46** 436–8

[46] Snyder D S and Small P L 2001 Staining of cellular mitochondria with LDS-751 *J. Immunol. Methods* **257** 35–40

[47] Xu L, Zhu Z, Wei D, Zhou X, Qin J and Yang C 2014 Amino-modified tetraphenylethene derivatives as nucleic acid stain: relationship between the structure and sensitivity *ACS Appl Mater Interfaces* **6** 18344–51

[48] Wishart D S, Feunang Y D, Guo A C, Lo E J, Marcu A, Grant J R, Sajed T, Johnson D, Li C, Sayeeda Z, Assempour N, Iynkkaran I, Liu Y, Maciejewski A, Gale N, Wilson A, Chin L, Cummings R, Le D, Pon A, Knox C and Wilson M 2018 DrugBank 5.0: a major update to the DrugBank database for 2018 *Nucleic Acids Res.* **46** D1074–82

[49] Quent V M, Loessner D, Friis T, Reichert J C and Hutmacher D W 2010 Discrepancies between metabolic activity and DNA content as tool to assess cell proliferation in cancer research *J Cell Mol Med* **14** 1003–13

[50] Zielonka J, Vasquez-Vivar J and Kalyanaraman B 2008 Detection of 2-hydroxyethidium in cellular systems: a unique marker product of superoxide and hydroethidine *Nat Protoc* **3** 8–21

[51] Canto M I 1999 Staining in gastrointestinal endoscopy: the basics *Endoscopy* **31** 479–86

[52] Badaro E, Novais E A, Penha F M, Maia M, Farah M E and Rodrigues E B 2014 Vital dyes in ophthalmology: a chemical perspective *Curr. Eye Res.* **39** 649–58

[53] Kirkpatrick N D, Zou C, Brewer M A, Brands W R, Drezek R A and Utzinger U 2005 Endogenous fluorescence spectroscopy of cell suspensions for

chemopreventive drug monitoring *Photochem. Photobiol.* **81** 125–34

[54] Stockman A, MacLeod D I A and Johnson N E 1993 Spectral sensitivities of the human cones *J. Opt. Soc. Am. A, JOSAA* **10** 2491–521

[55] Friedrich Menges 2018 *Spectragryph - optical spectroscopy software*

[56] Pawley J 2000 The 39 Steps: A Cautionary Tale of Quantitative 3-D Fluorescence Microscopy *BioTechniques* **28** 884–7

[57] Rueden C T, Schindelin J, Hiner M C, DeZonia B E, Walter A E, Arena E T and Eliceiri K W 2017 ImageJ2: ImageJ for the next generation of scientific image data *BMC Bioinformatics* **18** 529

[58] Stockert J C, Trigoso C I, Llorente A R and Del Castillo P 1991 DNA fluorescence induced by polymethine cation pyrvinium binding *Histochem. J.* **23** 548–52

[59] Nutrition C for F S and A 2019 Summary of Color Additives for Use in the United States in Foods, Drugs, Cosmetics, and Medical Devices *FDA*

[60] Pautke C, Vogt S, Kreutzer K, Haczek C, Wexel G, Kolk A, Imhoff A B, Zitzelsberger H, Milz S and Tischer T 2010 Characterization of eight different tetracyclines: advances in fluorescence bone labeling *J. Anat.* **217** 76–82

[61] Wittich C M, Burkle C M and Lanier W L 2012 Ten Common Questions (and Their Answers) About Off-label Drug Use *Mayo Clin Proc* **87** 982–90

[62] Polet H 1975 Role of the cell membrane in the uptake of 3H-actinomycin D by mammalian cells in vitro *J. Pharmacol. Exp. Ther.* **192** 270–9

[63] Feofanov A, Sharonov S, Kudelina I, Fleury F and Nabiev I 1997 Localization and molecular interactions of mitoxantrone within living K562 cells as probed by confocal spectral imaging analysis *Biophys. J.* **73** 3317–27

[64] Bell D H 1988 Characterization of the fluorescence of the antitumor agent, mitoxantrone *Biochim. Biophys. Acta* **949** 132–7

[65] Dixon J M, Taniguchi M and Lindsey J S 2005 PhotochemCAD 2: a refined program with accompanying spectral databases for photochemical calculations *Photochem. Photobiol.* **81** 212–3

[66] Bourassa P, Thomas T J and Tajmir-Riahi H A 2014 Locating the binding sites of antitumor drug tamoxifen and its metabolites with DNA *Journal of Pharmaceutical and Biomedical Analysis* **95** 193–9

[67] Weissig V, Lasch J, Erdos G, Meyer H W, Rowe T C and Hughes J 1998 DQAsomes: a novel potential drug and gene delivery system made from Dequalinium *Pharm. Res.* **15** 334–7

[68] Maltas E 2014 Binding interactions of niclosamide with serum proteins *J Food Drug Anal* **22** 549–55

[69] Wang Y-Q, Zhang H-M, Zhang G-C, Tao W-H and Tang S-H 2007 Interaction of the flavonoid hesperidin with bovine serum albumin: A fluorescence quenching study *Journal of Luminescence* **126** 211–8

[70] Motlagh N S H, Parvin P, Ghasemi F and Atyabi F 2016 Fluorescence properties of several chemotherapy drugs: doxorubicin, paclitaxel and bleomycin *Biomed Opt Express* **7** 2400–6

[71] U.S. National Library of Medicine Pyrvinium *TOXNET: Toxicology Data Network*

[72] Saraswati S, Alfaro M P, Thorne C A, Atkinson J, Lee E and Young P P 2010 Pyrvinium, a Potent Small Molecule Wnt Inhibitor, Promotes Wound Repair and Post-MI Cardiac Remodeling *PLOS ONE* **5** e15521

[73] Kömerik N, Curnow A, MacRobert A J, Hopper C, Speight P M and Wilson M 2002 Fluorescence Biodistribution and Photosensitising Activity of Toluidine Blue O on Rat Buccal Mucosa *Lasers Med Sci* **17** 86–92

[74] Vidal B de C and Mello M L S 2019 Toluidine blue staining for cell and tissue biology applications *Acta Histochem.* **121** 101–12

[75] Hu Z and Tong C 2007 Synchronous fluorescence determination of DNA based on the interaction between methylene blue and DNA *Anal. Chim. Acta* **587** 187–93

[76] Moser J, Boscá F, Lovell W W, Castell J V, Miranda M A and Hye A 2000 Photobinding of carprofen to protein *Journal of Photochemistry and Photobiology B: Biology* **58** 13–9

[77] Cech T and Pardue M L 1977 Cross-linking of DNA with trimethylpsoralen is a probe for chromatin structure *Cell* **11** 631–40

[78] Wittung P, Kim S K, Buchardt O, Nielsen P and Nordèn B 1994 Interactions of DNA binding ligands with PNA-DNA hybrids *Nucleic Acids Res.* **22** 5371–7

[79] Saffran W A, Goldenberg M and Cantor C R 1982 Site-directed psoralen crosslinking of DNA. *Proc Natl Acad Sci U S A* **79** 4594–8

[80] Ormond A B and Freeman H S 2013 Dye Sensitizers for Photodynamic Therapy *Materials (Basel)* **6** 817–40

[81] Ibbotson S 2018 Drug and chemical induced photosensitivity from a clinical perspective *Photochemical & Photobiological Sciences* **17** 1885–903

[82] Lugović-Mihić L, Duvančić T, Ferček I, Vuković P, Japundžić I and Ćesić D 2017 Drug-Induced Photosensitivity - a Continuing Diagnostic Challenge *Acta Clin Croat* **56** 277–83

[83] Golshani M R, Khoobehi B and Peyman G A 1993 Calcein: a new dye for evaluation of the blood-retinal barrier by fluorophotometry *Int Ophthalmol* **17** 349–53

[84] Maurya N, Maurya J K, Singh U K, Dohare R, Zafaryab M, Moshahid Alam Rizvi M, Kumari M and Patel R 2019 In Vitro Cytotoxicity and Interaction of Noscapine with Human Serum Albumin: Effect on Structure and Esterase Activity of HSA *Mol. Pharm.* **16** 952–66

[85] Zhou J, Gupta K, Aggarwal S, Aneja R, Chandra R, Panda D and Joshi H C 2003 Brominated derivatives of noscapine are potent microtubule-interfering agents that perturb mitosis and inhibit cell proliferation *Mol. Pharmacol.* **63** 799–807

[86] Zhuang Y, Cai X, Yu J and Ju H 2004 Flow injection chemiluminescence analysis for highly sensitive determination of noscapine *Journal of Photochemistry and Photobiology A: Chemistry* **162** 457–62

[87] Umezu K, Yuasa S, Sudoh A, Kikumoto R and Ichikawa A 1985 Inhibitory effect of tritoqualine (TRQ) on histamine release from mast cells *Jpn. J. Pharmacol.* **38** 153–60

[88] Allison A C 2005 Mechanisms of action of mycophenolate mofetil *Lupus* **14 Suppl 1** s2-8

[89] Ma X, Guo L, Wang Q, He J and Li H 2016 Spectroscopy and Molecular Modeling Study on the Interaction Between Mycophenolate Mofetil and Pepsin *J Fluoresc* **26** 599–608

[90] Voicescu M and Ionescu S 2014 Fluorescence characteristics of some flavones probes in different micellar media *J Fluoresc* **24** 735–43

[91] Culp S J and Beland F A 1996 Malachite Green: A Toxicological Review *Journal of the American College of Toxicology* **15** 219–38

[92] Shukla D, Kalliath J, Neelakantan N, Naresh K B and Ramasamy K 2011 A comparison of brilliant blue G, trypan blue, and indocyanine green dyes to assist internal limiting membrane peeling during macular hole surgery *Retina (Philadelphia, Pa.)* **31** 2021–5

[93] Frumovitz M, Plante M, Lee P S, Sandadi S, Lilja J F, Escobar P F, Gien L T, Urbauer D L and Abu-Rustum N R 2018 Near-infrared fluorescence for detection of sentinel lymph nodes in women with cervical and uterine cancers (FILM): a

randomised, phase 3, multicentre, non-inferiority trial *The Lancet Oncology* **19** 1394–403

[94] Enaida H and Ishibashi T 2008 Brilliant blue in vitreoretinal surgery *Dev Ophthalmol* **42** 115–25

[95] Islam A, Khan A and Rahman Z A 1990 Corneal vital staining with gentian violet *Bangladesh Med Res Counc Bull* **16** 70–4

[96] Yao L, Xue X, Yu P, Ni Y and Chen F 2018 Evans Blue Dye: A Revisit of Its Applications in Biomedicine *Contrast Media & Molecular Imaging*

[97] Ben-Dror S, Bronshtein I, Wiehe A, Röder B, Senge M O and Ehrenberg B 2006 On the correlation between hydrophobicity, liposome binding and cellular uptake of porphyrin sensitizers *Photochem. Photobiol.* **82** 695–701

[98] Khurana R, Uversky V N, Nielsen L and Fink A L 2001 Is Congo Red an Amyloid-specific Dye? *J. Biol. Chem.* **276** 22715–21

[99] Clement C G and Truong L D 2014 An evaluation of Congo red fluorescence for the diagnosis of amyloidosis *Hum. Pathol.* **45** 1766–72

[100] Monson F C, Wein A J, McKenna B A, Whitmore K and Levin R M 1991 Indigocarmine as a quantitative indicator of urothelial integrity *J. Urol.* **145** 842–5

[101] Snapp E L 2013 Chapter 12 - Photobleaching Methods to Study Golgi Complex Dynamics in Living Cells *Methods in Cell Biology* Methods for Analysis of Golgi Complex Function vol 118, ed F Perez and D J Stephens (Academic Press) pp 195–216